RSC Advances

PAPER

View Article Online
View Journal | View Issue

Cite this: *RSC Adv.*, 2024, **14**, 20300

DFT study of Ti_3C_2 MXene nanosheets as a drug delivery system for 5-fluorouracil†

Maryam Sadeghi and Bahram Khoshnevisan *

Received 29th March 2024
Accepted 12th June 2024

DOI: 10.1039/d4ra02399d

rsc.li/rsc-advances

In this study, we modeled a drug delivery system consisting of Ti_3C_2 MXene nanosheets as a carrier and 5-fluorouracil (FU) as a selected drug molecule using density functional theory (DFT) computations. During the adsorption procedure, electronic, magnetic and structural properties were calculated. Our results showed that the adsorption of FU drugs on the Ti_3C_2 surface is thermodynamically favorable. Our spin-polarized calculations also determined that the magnetization of Ti_3C_2 after FU adsorption does not change significantly, which is an important factor for magnetic hyperthermia and drug delivery. In addition, our calculations indicate that in the slightly acidic environment of tumor tissue, FU could start to be released (by increasing distance from the MXene surface and then instability of the complex) from the Ti_3C_2 surface without any substantial change in the structural properties. This study could provide a deep understanding of the interaction mechanism of 2-dimensional (2D) MXene materials with drugs at the atomistic scale and have an important contribution to the discovery and application of novel 2D materials as drug delivery systems.

1. Introduction

The use of nanotechnology can be a promising innovation and transformation in medicine and especially in the design of new drugs for cancer treatment. Specifically, 2D nanomaterials are interesting in the field of drug delivery due to their physical, chemical and biological properties that often differ from their bulk structure.[1–4] Graphene and its derivatives and some other layered materials for instance hexagonal boron nitride (hBN), transition metal dichalcogenides (TMDs), transition metal oxides (TMOs), and black phosphorus (BP) are used in nanomedicine.[5–10]

Another group of 2D layered materials discovered by two groups of researchers from Drexel University are MXenes.[11] The new family with the general formula of $M_{n+1}AX_n$ is called the MAX phase and includes carbide, nitride and carbonitride of transition metals. In this formula, M, A and X are: transition metal atom, a main group element (mostly group 13 or 14 element from the periodic table), and carbon or nitrogen atoms, respectively, and n can be 1 to 3. MXenes are obtained by the selective etching of the A-layers of the MAX phase either in pure form ($M_{n+1}X_n$), or with surface functional groups, $M_{n+1}X_nT_x$, where T_x can be fluorine (F), hydroxyl (OH) and oxygen(O).[12]

MXenes have excellent properties in terms of electrical, optical and thermal stability, so most conducted studies on them have focused on energy storage,[13,14] catalysis,[15] and sensors.[16,17] MXenes also have (i) high specific surface area, which is an efficient factor for high drug loading, (ii) tunable layered structure, and (iii) hydrophilic nature, which make them to be considered as new inorganic nanostructures for biological and biomedical applications.[18] MXenes also have high photothermal conversion efficiency, which makes these materials suitable for photothermal therapy and hyperthermia.[19,20]

Ti_3C_2 is the first MXene that was discovered in 2011 by Michael Naguib *et al.*[21] So far, many theoretical and experimental studies have been performed on it in various areas. In 2017 and 2020, A. M. Jastrzębska *et al.* investigated the cytotoxic effects of Ti_3C_2. The results revealed that these nanosheets exhibited the highest cytotoxic effect on the cancerous cell line of A549 while the normal cell line HaCaT showed no changes across all concentrations and remained unharmed.[22] Furthermore, they deposited a layer of Ti_2O_3 on the $Ti_3C_2T_x$ MXene using ultrasound and mild thermal oxidation after the synthesis process and indicated that it could probably regulate the cytotoxicity of samples to cancer cells. These samples were toxic to all cancer cell lines up to 375 mg l^{-1}.[23] In 2018, C. Xing *et al.* developed a MXene/DOX@cellulose hydrogel nano-platform, where MXene comprised Ti_3C_2 nanosheets, to study the release of the DOX model drug and its photothermal performance. This platform showed desirable biocompatibility, good photothermal efficiency and high capacity for Dox drug loading, and it was useful for immediate tumor destruction and preventing its recurrence.[24] For the first time, the performance of Ti_3C_2 MXene for chemotherapy drug delivery was investigated by X. Han in 2018. The drug was released by pH-responsive method and NIR laser technique, and a high synergistic

Faculty of Physics, University of Kashan, Kashan, Iran. E-mail: b.khosh@kashanu.ac.ir

† Electronic supplementary information (ESI) available. See DOI: https://doi.org/10.1039/d4ra02399d

therapeutic outcome was obtained in the treatment of cancer.[25] G. Liu *et al.* used a multifunctional nanoplatform (Ti_3C_2–DOX), in which the nanosheets have a small lateral size (~100 nm) and included the stable surface functional group $Al(OH)_4$. The work offered a new effective strategy for cancer therapy based on surface-modified Ti_3C_2 nanosheets.[26] B. Zhu *et al.* combined gold nanorods (GNRs) with Ti_3C_2 nanosheets and prepared intelligent sandwich-like Ti_3C_2@GNRs/PDA/Ti_3C_2 nanohybrids, which were used for drug delivery with synergistically enhanced NIR drug release behavior. The results showed that this platform had pH/NIR-responsive drug release. Overall, it was promising for use in photothermal therapy and in remote controllable drug delivery.[27] In 2020, Y. Liu *et al.* developed a heterostructured titanium carbide–cobalt nanowires (Ti_3C_2–CoNWs) nanocarrier. When DOX was used as a model drug, this nanocarrier had a high drug loading ability and showed drug release behavior induced by pH/NIR stimulations.[28] In 2023, Z. Bai *et al.* showed that under the irradiation of a NIR-I laser, the Ti_3C_2 core in the DOX/Ti_3C_2/Apt-M therapeutic platform enhanced the effect of PTT and promoted the release of the DOX to enhance the chemotherapy effect.[29]

To the best of our knowledge, theoretical calculations have not been reported so far on using Ti_3C_2 as a drug delivery system for fluorouracil. Fluorouracil (abbreviated: 5-FU or FU) is one of the common cancer treatment drugs for some cancers, such as breast, stomach and colon.[30]

In this work, based on Density Functional Theory (DFT), we have modeled Ti_3C_2 MXene nanosheets as a carrier for FU. First, we investigated the adsorption behavior of 5-FU on Ti_3C_2 nanosheets. Then, we calculated the electronic structure and magnetic properties of Ti_3C_2@FU systems. Finally, drug release from the carrier surface, which is an important part of the drug delivery process, has been investigated. We hope this study provides a deep understanding of the interaction mechanism at the atomistic scale, and provides some insight for biomedical applications of Ti_3C_2 MXene nanosheets.

2. Computational methods

The calculations were done based on density functional theory (DFT) using the Quantum-ESPRESSO package. The exchange correlation interaction was considered within the generalized gradient approximation (GGA), Perdew–Burke–Ernzerhof (PBE).[31,32] The vacuum space was considered to be 25 Å along the *z*-direction to prevent interaction with the periodic image of nanosheets. The energy cutoff for plane waves was set to 480 eV, and the convergence in energy and force were 10^{-4} eV and 10^{-4} eV Å^{-1}, respectively. The van der Waals interactions, as a semiempirical correction, were also added through the "DFT-D2" treatment suggested by Grimme.[33,34]

3. Result and discussion

3.1 Structural properties of Ti_3C_2 and FU

In our study, Ti_3C_2 MXene nanosheets serve as the drug carrier. To simulate the primary structure of this MXene, its bulk structure was used as a model and a relaxation calculation was then performed for the Ti_3C_2 monolayer. Fig. 1 shows the Ti_3C_2 monolayer structure. The single layer of Ti_3C_2 includes two of the same groups of Ti atoms in the upper and lower regions of the layer, and one row of Ti atoms in the center that we will call Ti_1 and Ti_2, respectively (Fig. 1). It should be noted that Ti_1 and Ti_2 are different in magnetic and electronic properties.[35] There are two rows of C atoms in the middle of the titanium atoms that bonded with Ti_1 and Ti_2.

In the relaxed structure of the Ti_3C_2 monolayer, the *a*-lattice parameter of its hexagonal structure was determined to be 3.07 Å, and the bond lengths of Ti_1–C and Ti_2–C were found to be 2.05 and 2.20 Å, respectively. The thickness of the sheet (distance between Ti_1 atoms at the upper and lower level of the surface) was 4.72 Å. For comparison, other theoretical and experimental results are summarized in Table 1, and it can be seen that our results are in good agreement with them.[36–48]

FU is one of the common drugs used to treat cancer and has five different structures: the Diketo (contains two carbonyl groups), Dienol (contains two hydroxyl groups), and three Ketoenol tautomers (with one carbonyl and one hydroxyl groups). We have investigated all five structures in our simulations. It also must be noted that Ketoenol has three different configurations, and we took the most stable of them in our study (Fig. 2).[49,50]

At first, each structure was simulated and optimized, and the bond lengths after relaxation calculations for each of the three

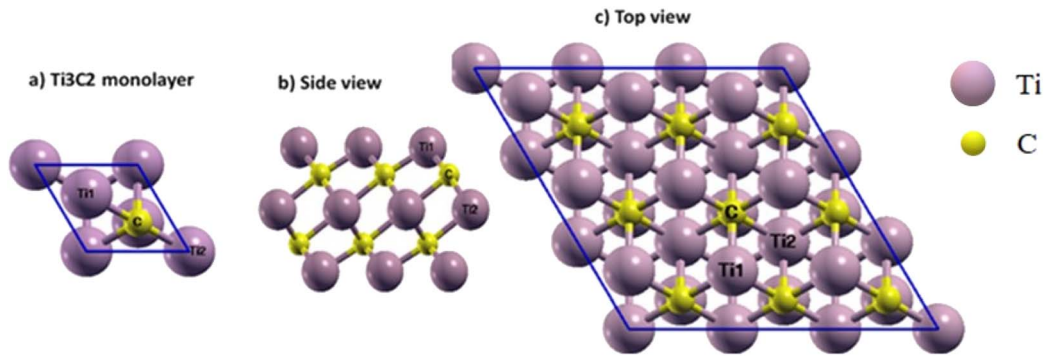

Fig. 1 (a) Ti_3C_2 unit cell, (b) side and (c) top views of the 3 × 3 × 1 supercell of Ti_3C_2 MXene. Three special sites for the absorption process are marked on the (c).

Table 1 Structural properties and magnetization of Ti_3C_2[a]

	a (Å)	Ti_1–C (Å)	Ti_2–C (Å)	Thickness (Å)	Magnetization (μ_B)
This work	3.07	2.05	2.20	4.72	1.85
Other reports	3.07 (ref. 36 and 48)	2.064 (ref. 47)	2.21 (ref. 36)	4.66 (ref. 36)	1.9 (ref. 36), 1.93 (ref. 47)
	3.10 (ref. 46)	2.062 (ref. 37)	2.22 (ref. 37)	4.64 (ref. 37)	1.87 (ref. 38)
	3.08 (ref. 39)	2.083 (ref. 39)	2.21 (ref. 40)	4.60 (ref. 41)	2.2 (ref. 42)
	*3.08 (ref. 43), *3.09 (ref. 44)				*1.87 (ref. 39 and 45)

[a] * means experimental reports.

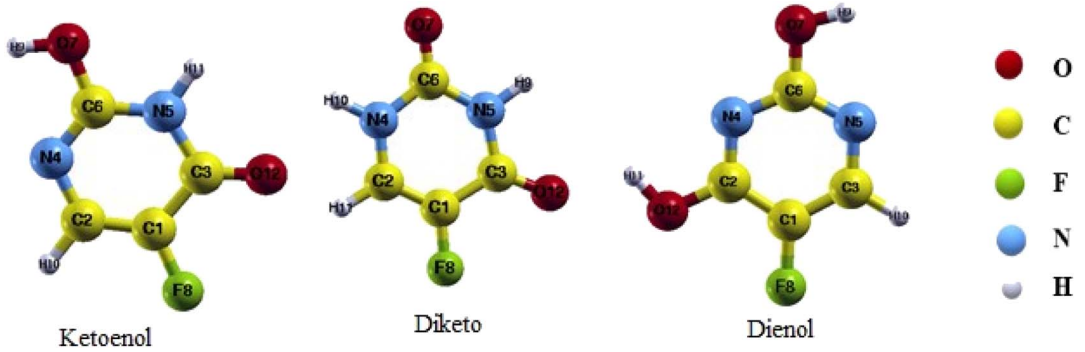

Fig. 2 Different structures of the 5-FU drug.

drug forms are given in the first row of Tables 2–4. In comparison with the literature, there is a good agreement between our results and the previous theoretical and experimental reports.[51–53]

3.2 FU adsorption on the Ti_2C_3 surface (Ti_3C_2@ FU)

To consider the FU adsorption on the Ti_2C_3 surface, we made a 3 × 3 × 1 supercell of Ti_3C_2. It is well known that according to the crystal structural symmetry of the Ti_3C_2 sheet, there are three adsorption sites for adding drugs and they are marked in Fig. 1.[47,54] The first site is on the top of the Ti atom on the surface ($\perp_{Ti_1}$), the second is above the C atoms ($\perp_C$) and the last one is on the top of the middle row of Ti atoms ($\perp_{Ti_2}$).

The selected drug molecules were approached to the Ti_3C_2 surface at the $\perp_{Ti_1}$, $\perp_{Ti_2}$ and $\perp_C$ sites. For example, Fig. 3 displays the most stable Ti_3C_2@ FU systems before and after the

Table 2 The bond lengths of Diketo. Rows 3–5 show the band lengths after Diketo adsorption on Ti_3C_2 at $\perp_{Ti_1}$, $\perp_{Ti_2}$ and $\perp_C$ configurations. Row 6 displays the bond lengths after Diketo release from the surface

	N5–H9	C3–O12	C1–F8	C2–H11	N4–H10	C6–O7	C6–N5	N5–C3	C3–C1	C1–C2	C2–N4	N4–C6
Diketo	1.01	1.23	1.35	1.09	1.01	1.22	1.39	1.40	1.46	1.35	1.37	1.39
Ref. 51	—	1.22	1.34	—	—	1.22	1.40	1.40	1.47	1.35	1.38	1.39
$\perp_{Ti_1}$	1.02	1.23	1.37	1.09	1.01	1.22	1.39	1.40	1.45	1.35	1.37	1.39
$\perp_{Ti_2}$	Not converge	—	—	—	—	—	—	—	—	—	—	—
$\perp_C$	1.02	1.31	1.37	1.08	1.01	1.22	1.39	1.39	1.40	1.36	1.39	1.39
After release $\perp_C$	1.02	1.31	1.36	1.08	1.01	1.22	1.39	1.38	1.41	1.36	1.38	1.39

Table 3 The bond lengths of Ketoenol. Rows 3–5 list the bonds lengths after Ketoenol adsorption on Ti_3C_2 at the $\perp_{Ti_1}$, $\perp_{Ti_2}$ and $\perp_C$ configurations. Row 6 displays the bond lengths after Ketoenol release from the surface

	H9–O7	O7–C6	C6–N5	N5–C3	C3–C1	C1–C2	C2–N4	N4–C6	C2–H10	C1–F8	C3–O12	N5–H11
Ketoenol	0.98	1.35	1.36	1.42	1.45	1.36	1.37	1.30	1.09	1.35	1.23	1.02
Ref. 52 and 53	0.98	1.34	1.36	1.42	—	1.37	—	1.30	—	1.35	1.22	1.02
$\perp_{Ti_1}$	0.98	1.34	1.36	1.42	1.44	1.36	1.37	1.30	1.09	1.38	1.23	1.02
$\perp_{Ti_2}$	0.98	1.35	1.36	1.42	1.44	1.36	1.37	1.30	1.09	1.37	1.23	1.02
$\perp_C$	0.98	1.34	1.36	1.42	1.45	1.36	1.37	1.30	1.09	1.36	1.23	1.02
After release $\perp_C$	0.98	1.34	1.36	1.4	1.45	1.36	1.37	1.3	1.1	1.35	1.23	1.02

Table 4 The bond lengths of Dienol and its comparison with experimental reports. Rows 3 – 5 list the bonds lengths after Dienol adsorption on Ti_3C_2 at $\perp_{Ti_1}$, $\perp_{Ti_2}$ and $\perp_C$ configurations. Row 6 displays the bond lengths after Dienol release from the surface

	H9–O7	O7–C6	C6–N4	N4–C2	C2–O12	O12–H11	C2–C1	C1–C3	C1–F8	C3–H9	C3–N5	N5–C6
Dienol	0.98	1.35	1.33	1.33	1.34	0.98	1.40	1.38	1.35	1.09	1.34	1.34
Ref. 52 and 53	0.98	1.35	1.34	1.33	—	—	—	1.38	1.35	—	—	1.34
$\perp_{Ti_1}$	0.98	1.34	1.34	1.32	1.34	0.98	1.40	1.38	1.38	1.09	1.34	1.34
$\perp_{Ti_2}$	0.98	1.34	1.33	1.32	1.36	0.10	1.39	1.38	1.38	1.09	1.34	1.34
$\perp_C$	0.98	1.34	1.34	1.32	1.34	0.98	1.40	1.38	1.38	1.09	1.34	1.34
After release $\perp_{Ti_2}$	0.98	1.35	1.34	1.33	1.35	0.98	1.40	1.38	1.36	1.09	1.34	1.34

relaxation calculations, and other configurations before and after the relaxation can be seen in Fig. 1S–3S in the ESI† Section (Appendix). In the cases of Ketoenol and Diketo, $\perp_C$ is the most stable configuration. Meanwhile, in the Dienol case, $\perp_{Ti_2}$ is the most stable site for the drug. The bond lengths of the drug molecules after adsorption were calculated and are summarized in Tables 2–4. It can be seen that the bond lengths of the drugs have not changed after adsorption, which confirmed that the structures of the drugs were preserved.

In order to obtain the most stable structure, the adsorption energy was calculated for each of the three configurations. The formula for calculating adsorption energy is:

$$E_{ad} = (E_{Ti_3C_2@FU}) - (E_{Ti_3C_2} - E_{FU}) \quad (1)$$

On the right side of the equation, the first term expresses the energy of the optimized Ti_3C_2@FU complex. The second ($E_{Ti_3C_2}$) and third (E_{FU}) terms are the Ti_3C_2 energy and free drug energy after optimization, respectively.

The structure with the highest negative adsorption energy was known as the most stable Ti_3C_2@drug system. Table 5 shows the calculated adsorption energies of each structure in the considered adsorption sites. E_{ad} of the Diketo on the $\perp_C$ site was calculated to be −3.39 eV, which is the most stable system. Moreover, $\perp$the Ti2 site was the most stable configuration for Dienol with E_{ad} equal to −2.36 eV. For Ketoenol, the $\perp_C$ site with E_{ad}: −2.03 eV was the most stable structure.

We compared our results with literature (Table 6), and our calculated E_{ad} were higher than the adsorption of the FU drug on some nanosheets, such as SiG, BN, InN, AlN, ZnO, SWCNTs and also BNNT.[50,55–60] In these nanosheets and nanotubes, it is necessary to increase the adsorption energy using some process such as doping because the E_{ad} is low. On the other hand, our results were lower than those from the Diketo adsorption on GaN.[62] In this case, there are problems with the drug releasing procedure. Our E_{ad} were comparable with FU adsorbed on GNS and in some sites on graphene oxide, respectively.[61,63]

3.3 Electronic and structural stability properties

Furthermore, the electronic density of state (DOS) is the main criterion for better understanding what happens during the drug interaction with the carrier surface. For this purpose, the DOS was calculated for the Ti_3C_2@FU systems. Furthermore, the DOS diagrams of bare Ti_3C_2 and FU were plotted for comparison.

Fig. 4 shows the results of the partial DOS and total DOS diagrams of the Ti_3C_2@FU complexes. A careful comparison between the DOS of Ti_3C_2 and Ti_3C_2@FU systems reveals that the insertion of a drug into Ti_3C_2 altered the amount of the DOS at the Fermi surface. Actually, the amount of DOS at the Fermi surface increased slightly with respect to the Ti_3C_2 surface; these new states belonged to the drugs. Further investigation showed that the partial DOS of the drugs did not change after adsorption. This means that the electronic properties of the drug were slightly affected during the interaction, and it can be said that the structure of the drug was preserved during the adsorption.

The DOS diagram of the bare Ti_3C_2 shows the metallic behavior, and the Ti_1 atoms have the main contribution on the Fermi level (Fig. 4a).

The molecular structure stability and reactivity could be predicted by chemical potential and chemical hardness. We have calculated the chemical potential and hardness using the following equations:

$$\mu = \frac{E_{LUMO} + E_{HOMO}}{2} \quad (2)$$

$$\eta = \frac{E_{LUMO} - E_{HOMO}}{2} \quad (3)$$

where μ is the electronic chemical potential and η is the chemical hardness of the ground state.[45,64] E_{HOMO} is the energy of the highest occupied molecular orbital and E_{LUMO} is the energy of the lowest unoccupied molecular orbital of the considered structures.

The results are shown in Table 7. It is found that after the adsorption, the values of the HOMO–LUMO energy gap (H/L gap) and chemical hardness for all of the systems were reduced. This indicated that the chemical stability of the drugs would be diminished; therefore, its chemical activity would be increased.

To consider the charge transfer between the Ti_3C_2 surface and adsorbed drug molecule, we also calculated the ΔN parameter, which shows the fractional electron's charge that transfers from system A to system B:

$$\Delta N = (\mu_B - \mu_A)/(\eta_B + \eta_A) \quad (4)$$

where $\eta_{A(B)}$ and $\mu_{A(B)}$ are the chemical hardness and chemical potential of the acceptor (donor), respectively. As shown in Table 7, the values of ΔN are positive, indicating that the charge

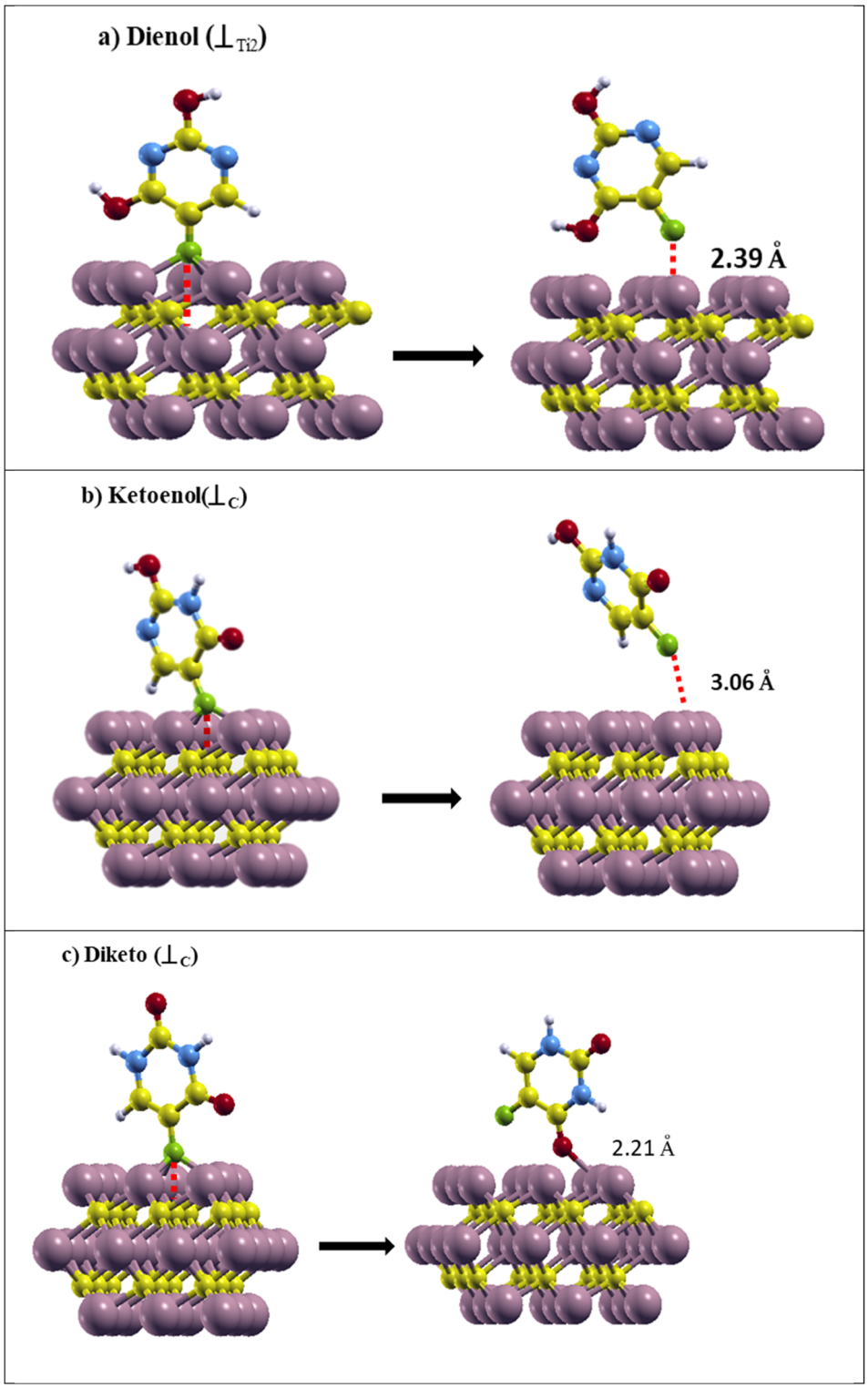

Fig. 3 (a) Ti_3C_2@Dienol, (b) Ti_3C_2@Ketoenol, and (c) Ti_3C_2@Diketo before (left) and after (right) the adsorption process in the most stable configurations.

flowed from the surface to drugs so Ti_3C_2 was the donor and the added molecules were the acceptor.

Iso surfaces of the most stable structures are also shown in Fig. 5. We can see the charge transfer between the drug and the surface during the adsorption process, which implied the interaction between the adsorbent and the surface in each of the three states.

Table 5 E_{ad} (eV) at the selected sites after optimization of all geometries of the Ti_3C_2@FU complex

	Ti_3C_2@Diketo	Ti_3C_2@Ketoenol	Ti_3C_2@Dienol
$\perp_C$	−3.39	−2.03	−2.01
$\perp_{Ti_2}$	Not converged	−1.94	−2.36
$\perp_{Ti_1}$	−2.01	−1.99	−2.01

Table 7 HOMO and LUMO and H/L gap for the most stable optimized nanocages structures

	HOMO (eV)	LUMO (eV)	H/L gap	η (eV)	η (eV)	ΔN
Ti_3C_2 surface	1.31	1.32	0.01	0.005	1.32	
Diketo ($\perp_C$)	2.09	2.09	0.00	0.002	2.09	3.05
Ketoenol ($\perp_C$)	2.006	2.009	0.003	0.002	2.08	2.80
Dienol ($\perp_{Ti_2}$)	2.10	2.11	0.01	0.005	2.11	2.68

3.4 Magnetic properties

The magnetic property is one of the most important features for drug delivery in order to achieve magnetic fluid hyperthermia. In this regard, the ideal nanoparticles for magnetic hyperthermia should show a satisfactory heating value at low magnetic fields, where the heating power is proportional to the magnetization squared.

To explore the magnetic behavior of Ti_3C_2 during the adsorption process, we performed spin-polarized density functional theory calculations. The total magnetic moment of the $3 \times 3 \times 1$ supercell of the Ti_3C_2 surface was calculated to be 20.28 μ_B per cell. Conversely, the average magnetic moment of each Ti_1 atom on the Ti_3C_2 surface was about 0.49 μ_B. For Ti_2 atoms in the middle of the surface, the calculated value was ~0.024 μ_B, which confirms that the magnetic properties of Ti_3C_2 are primarily due to the Ti_1 atoms.[35,47,65,66]

Table 6 Comparison of the adsorption energy of different forms of the FU drug on the different carrier surfaces

E_{ad} (eV)	Carrier surface	Form of FU drug	Ref.
−0.083, −0.172, −0.082	(SiG) silicon graphene nanosheet	Diketo/Ketoenol/Dienol	50
−0.56	BNNS (boron nitride nanosheet)	Diketo	55, and 56
−1.3, 0.81, −0.84	InN, AlN, GaN (nanosheet)	Diketo	55
−0.423	ZnONS (zinc oxide nanosheet)	Diketo	57
−0.358	(4,0) SWCNT	Diketo	58
−0.13	(8,0) BNNT (boron nitride nanotube)	Diketo	59, and 60
−1.74	(GONS) graphene oxide nanosheets	Diketo	61
−5.41, −4.29, −1.37	(GaN) gallium nitride	Diketo/Ketoenol/Dienol	62
−3.116	GNS (graphene nanosheet)	Diketo	63

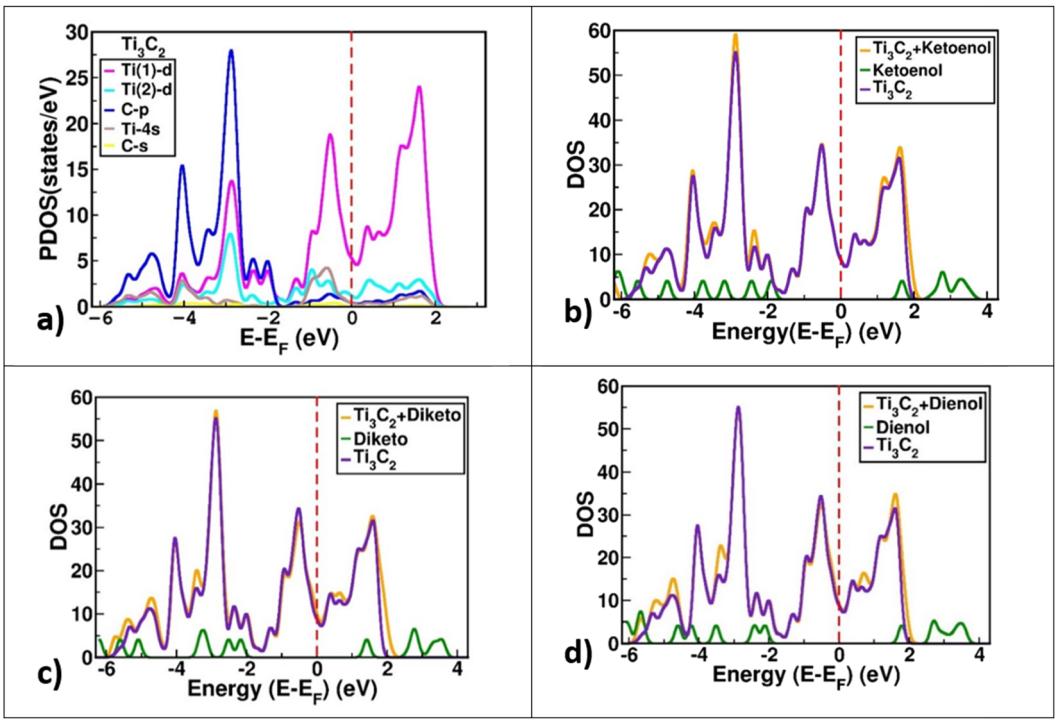

Fig. 4 (a) The partial density of state (PDOS) of the optimized Ti_3C_2 MXene. (b–d) The density of state (DOS) of the Ti_3C_2@FU surface complex.

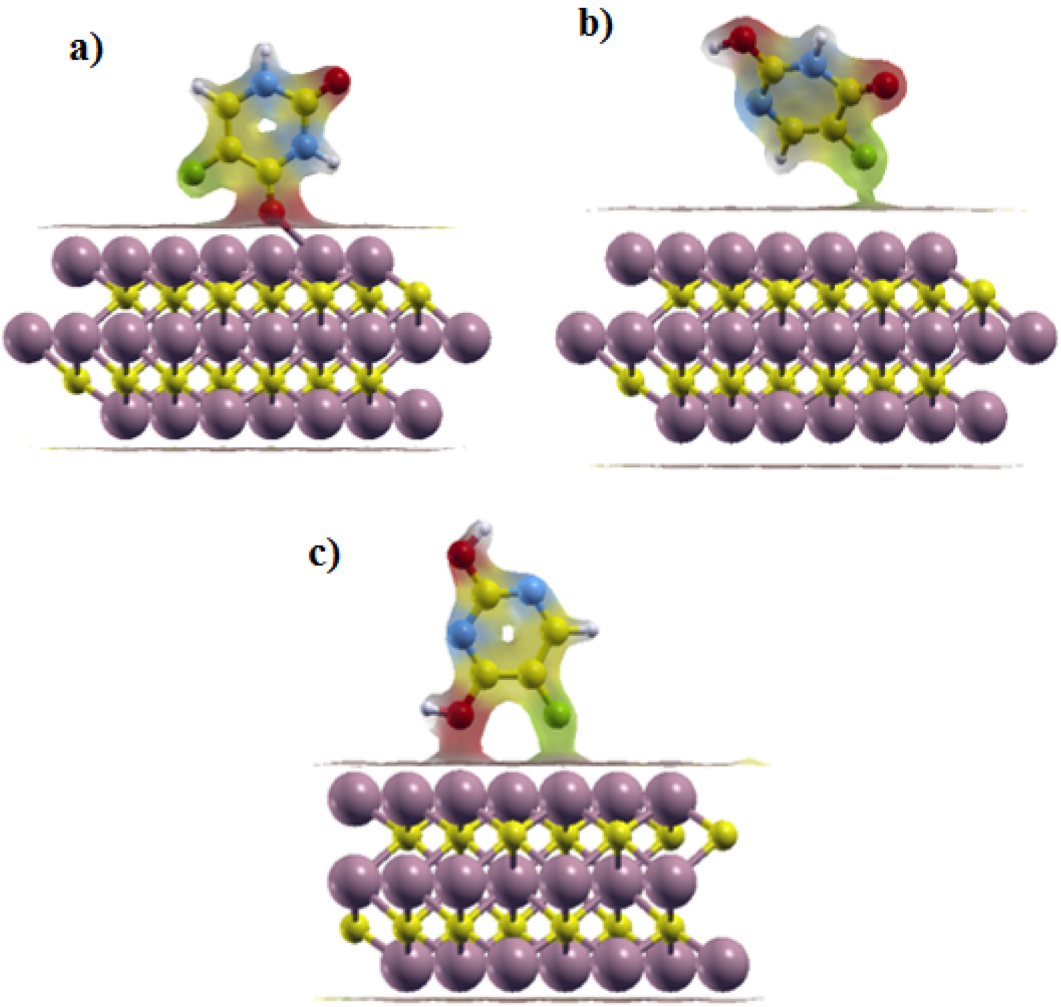

Fig. 5 Iso surfaces of the most stable structures: (a) Ti_3C_2@Diketo, (b) Ti_3C_2@Ketonel and (c) Ti_3C_2@Dienol.

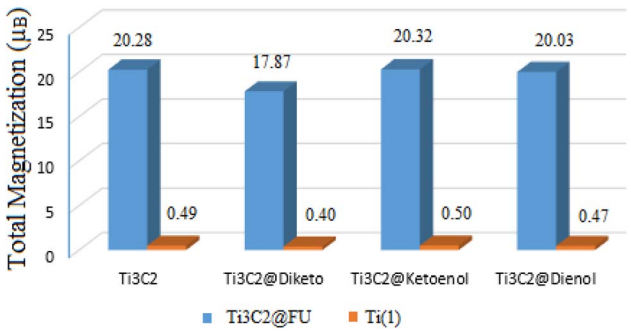

Fig. 6 Total magnetic moment of the Ti_1 atom and Ti_3C_2@FU systems at the most stable adsorption sites.

Fig. 6 shows the total magnetic moment of the most stable Ti_3C_2@FU systems. As it can be seen, the total magnetic moments varied in the range of 17.87 to 20.32 μ_B per cell. For the Ti_3C_2@Ketonel and Ti_3C_2@Dienol systems, the total magnetic moment did not change significantly before and after drug adsorption. In other words, drug adsorption did not destroy the magnetic properties of these systems. For the Ti_3C_2@Diketo case on the $\perp_C$ site of the surface, the total magnetic moment value decreased to 17.82 μ_B per cell. Ti_3C_2@Diketo has the highest E_{ad}. The oxygen atom of the Diketo bonded with one of the surface titanium atoms during the adsorption process, and caused the decrease of the magnetization. In contrast, for the two former cases, there was not any oxygen atom interactions. So, the bonding state plays a key role in the magnetic moment values. In all cases, after the drug adsorption on the carrier surface, in spite of the Ti_1 atoms being around the drug adsorption site, the value of the magnetic moment of the other Ti_1 atoms did not change significantly. However, Ti_1 atoms that were located around the drug adsorption site on the surface during the adsorption process showed a change in the range of 0.33 to 0.55 μ_B.

3.5 Drug release

The release of the drug from the carrier inside the target cells is the most vital step during the drug delivery process. In order to consider the Ti_3C_2 surface as a candidate for a drug delivery system, the drug release process had to be investigated. In the literature, the NIR laser was introduced as one method in this regard. However, in this work, we used the feature of the

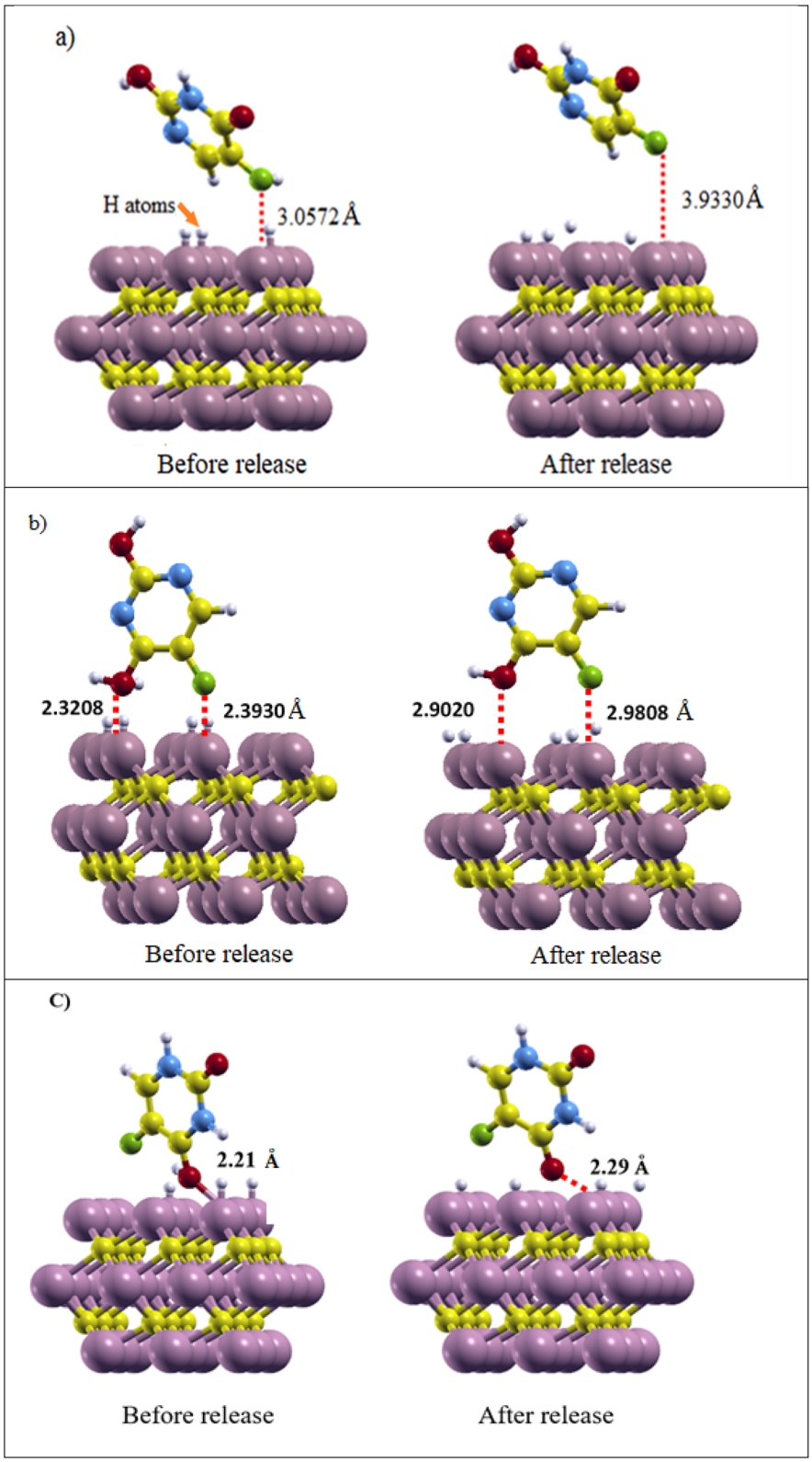

Fig. 7 (a) Ti_3C_2@Ketonel, (b) Ti_3C_2@Dienol, and (c) Ti_3C_2@Diketo before and after drug release. The distance of the drug from the surface and its amount before and after release is shown.

microenvironment inside the tumor, which has a lower pH than the surrounding healthy tissues.[25,28,67] For this reason, we calculated the release energy of the drug by adding protons around the binding site in the complex of the drug and the surface to weaken them. This could happen by adsorbing the free protons from the tumor matrix.

The added protons can attack different places of the complex, including nucleophilic and the other sites as well.[56,68] Therefore, we investigated the drug release behavior by considering the protons' attack on the drug, as well as the carrier surface around the adsorption site in the most stable structures.

In our modeling, the numbers of hydrogen atoms were added first to the F atom of the drug, but there was no sign of drug release. Therefore, we concluded that to weaken the surface Ti bindings with the drug, they should be attacked with protons gradually until the release features have been started.

The proton number was selected based on the sites expected to impact the release process, and the release energy was calculated per proton. According to the calculations in Section 3.3, it can be expected that the added protons and the carrier surface interact with each other. The charge is transferred from the surface to the protons, weakening (or breaking) the bond between the drug and the surface. After relaxation calculation of the Ti_3C_2@FU systems (Fig. 7), the calculated drug release energy was as follows: for the Ketoenol form in the $\perp_C$ state, the release energy was obtained at +1.75 eV and the distance of the drug from the surface during the structural optimization was increased by 0.87 Å. The F bond with the Ti_3C_2 surface weakened and finally broke, which gave rise to the release of Ketoenol from the Ti_3C_2 surface.

In Dienol in the $\perp_{Ti_2}$ state, due to the fact that the O atom is closer to the surface than the F atom, a hydrogen atom was added to the oxygen of the drug and the Ti atoms around it so the following release energy was obtained: +1.47 eV. The distance of the O atom from the Ti_3C_2 MXene surface increased from 2.32 to 2.90 Å and the F atom from 2.39 to 2.98 Å. Therefore, Dienol starts to be released in the slightly acidic environment of the tumor tissue, which reduces the toxins and side effects of this drug. In the Diketo form in the $\perp_C$ state, the distance of drug from Ti_3C_2 surface change about 0.08 Å with the change of the environment pH and release energy was obtained +1.57 eV, and it can be said that the release process has been started.

During the release of the drug from the carrier, the added protons approach the Ti_3C_2 nanosheets, which shows that the hydrogen atoms tend to interact with Ti atoms of the surface so the binding strength of these atoms with the drug could be weakened, respectively.

In order to ensure that the structure of the drug has not changed after release, the bond lengths of the drugs are compared with its the optimal model. The results are represented in row 6 of Tables 2–4. Our results showed that the structures of the drugs were not changed, so the properties of the drugs were preserved.

4. Conclusion

We modeled a drug delivery system consisting of Ti_3C_2 MXene nanosheets as a carrier and FU as a selected drug molecule using the quantum espresso computing package. In this study, the adsorption energies of different forms of the FU drug on the Ti_3C_2 carrier surface were calculated.

Our calculations confirm the stability of the Ti_3C_2@FU systems and exothermic interaction between FU and the Ti_3C_2 surface. Furthermore, charge flows from the Ti_3C_2 surface to drugs during the adsorption process. The amount of Ti_3C_2 surface DOS at the Fermi surface increases slightly after drug adsorption. The total magnetic moment of the $3 \times 3 \times 1$ supercell of the Ti_3C_2 surface was calculated to be 20.28 μ_B per cell. For the Ti_3C_2@Ketonel and Ti_3C_2@Dienol systems, the total magnetic moment did not change significantly with respect to that of Ti_3C_2, so drug adsorption did not destroyed the magnetic properties of these systems. However, for the Ti_3C_2@Diketo case, the total magnetic moment value decreased to 17.82 μ_B per cell.

Drug release can be achieved in the low pH environment of cancerous cells; the release energy was obtained at +1.75, +1.47 and +1.57 eV for Ketoenol, Dienol and Diketo, respectively. Results of the calculations provide a deep understanding of the interaction mechanism of 2D MXene materials with drugs at the atomistic scale.

Author contributions

M. Sadeghi: (PhD student) performed research, modeling and calculations, writing draft version. B. Khoshnevisan: (supervisor) designed research, grant holder, modeling, data analysis.

Conflicts of interest

The authors declare that they have no known competing financial interests or personal relationships that could have appeared to influence the work reported in this paper.

References

1 P. Boisseau and B. Loubaton, "Nanomedicine, nanotechnology in medicine", *C. R. Phys.*, 2011, **12**(7), 620–636.
2 H. Zhang, T. Fan, W. Chen, Y. Li and B. Wang, "Recent advances of two-dimensional materials in smart drug delivery nano-systems", *Bioact. Mater.*, 2020, **5**(4), 1071–1086.
3 J. Damodharan, "Nanomaterials in medicine–An overview", *Mater. Today: Proc.*, 2021, **37**, 383–385.
4 R. Davis Jr, R. A. Urbanowski Jr and A. K. Gaharwar, "2D layered nanomaterials for therapeutics delivery", *Curr. Opin. Biomed. Eng.*, 2021, **20**, 100319.
5 K. S. Novoselov, A. K. Geim, S. V. Morozov, D. E. Jiang, Y. Zhang, S. V. Dubonos, I. V. Grigorieva and A. A. Firsov, "Electric field effect in atomically thin carbon films", *Science*, 2004, **306**(5696), 666–669.
6 F. Nasrollahi, J. Varshosaz, A. A. Khodadadi, S. Lim and A. Jahanian-Najafabadi, "Targeted delivery of docetaxel by use of transferrin/poly (allylamine hydrochloride)-functionalized graphene oxide nanocarrier", *ACS Appl. Mater. Interfaces*, 2016, **8**(21), 13282–13293.
7 M. Vatanparast and Z. Shariatinia, "Hexagonal boron nitride nanosheet as novel drug delivery system for anticancer drugs: Insights from DFT calculations and molecular

dynamics simulations", *J. Mol. Graphics Modell.*, 2019, **89**, 50–59.

8 X. Zhou, H. Sun and X. Bai, "Two-dimensional transition metal dichalcogenides: synthesis, biomedical applications and biosafety evaluation", *Front. bioeng. biotechnol.*, 2020, **8**, 236.

9 D. Zeng, L. Wang, L. Tian, S. Zhao, X. Zhang and H. Li, "Synergistic photothermal/photodynamic suppression of prostatic carcinoma by targeted biodegradable MnO2 nanosheets", *Drug Delivery*, 2019, **26**(1), 661–672.

10 F. Wu, M. Zhang, X. Chu, Q. Zhang, Y. Su, B. Sun, T. Lu, N. Zhou, J. Zhang, J. Wang and X. Yi, "Black phosphorus nanosheets-based nanocarriers for enhancing chemotherapy drug sensitiveness *via* depleting mutant p53 and resistant cancer multimodal therapy", *Chem. Eng. J.*, 2019, **370**, 387–399.

11 M. Naguib, M. Kurtoglu, V. Presser, J. Lu, J. Niu, M. Heon, L. Hultman, Y. Gogotsi and M. W. Barsoum, "Two-dimensional nanocrystals produced by exfoliation of Ti3AlC2", *Adv. Mater.*, 2011, **23**(37), 4248–4253.

12 M. Alhabeb, K. Maleski, B. Anasori, P. Lelyukh, L. Clark, S. Sin and Y. Gogotsi, "Guidelines for synthesis and processing of two-dimensional titanium carbide (Ti3C2T x MXene)", *Chem. Mater.*, 2017, **29**(18), 7633–7644.

13 X. Zhang, Z. Zhang and Z. Zhou, "MXene-based materials for electrochemical energy storage", *J. Energy Chem.*, 2018, **27**(1), 73–85.

14 E. M. Siriwardane, I. Demiroglu, C. Sevik, F. M. Peeters and D. Çakır, "Assessment of Sulfur-functionalized MXenes for Li-ion Battery applications", *J. Phys. Chem. C*, 2020, **124**(39), 21293–21304.

15 Z. W. Seh, K. D. Fredrickson, B. Anasori, J. Kibsgaard, A. L. Strickler, M. R. Lukatskaya, Y. Gogotsi, T. F. Jaramillo and A. Vojvodic, "Two-dimensional molybdenum carbide (MXene) as an efficient electrocatalyst for hydrogen evolution", *ACS Energy Lett.*, 2016, **1**(3), 589–594.

16 S. J. Kim, H. J. Koh, C. E. Ren, O. Kwon, K. Maleski, S. Y. Cho, B. Anasori, C. K. Kim, Y. K. Choi, J. Kim and Y. Gogotsi, "Metallic Ti3C2T x MXene gas sensors with ultrahigh signal-to-noise ratio", *ACS Nano*, 2018, **12**(2), 986–993.

17 D. H. Ho, Y. Y. Choi, S. B. Jo, J. M. Myoung and J. H. Cho, "Sensing with MXenes: progress and prospects", *Adv. Mater.*, 2021, **33**(47), 2005846.

18 H. Lin, Y. Chen and J. Shi, "Insights into 2D MXenes for versatile biomedical applications: current advances and challenges ahead", *Adv. Sci.*, 2018, **5**(10), 1800518.

19 W. Tang, Z. Dong, R. Zhang, X. Yi, K. Yang, M. Jin, C. Yuan, Z. Xiao, Z. Liu and L. Cheng, "Multifunctional two-dimensional core–shell mxene@ gold nanocomposites for enhanced photo–radio combined therapy in the second biological window", *ACS Nano*, 2018, **13**(1), 284–294.

20 H. Lin, X. Wang, L. Yu, Y. Chen and J. Shi, "Two-dimensional ultrathin MXene ceramic nanosheets for photothermal conversion", *Nano Lett.*, 2017, **17**(1), 384–391.

21 M. Naguib, O. Mashtalir, J. Carle, V. Presser, J. Lu, L. Hultman, Y. Gogotsi and M. W. Barsoum, "Two-dimensional transition metal carbides", *ACS Nano*, 2012, **6**(2), 1322–1331.

22 A. M. Jastrzębska, A. Szuplewska, T. Wojciechowski, M. Chudy, W. Ziemkowska, L. Chlubny, A. Rozmysłowska and A. Olszyna, "*In vitro* studies on cytotoxicity of delaminated Ti3C2 Mxene", *J. Hazard. Mater.*, 2017, **339**, 1–8.

23 A. M. Jastrzębska, A. Szuplewska, A. Rozmysłowska-Wojciechowska, M. Chudy, A. Olszyna, M. Birowska, M. Popielski, J. A. Majewski, B. Scheibe, V. Natu and M. W. Barsoum, "On tuning the cytotoxicity of Ti3C2 (MXene) flakes to cancerous and benign cells by post-delamination surface modifications", *2D Mater.*, 2020, **7**(2), 025018.

24 C. Xing, S. Chen, X. Liang, Q. Liu, M. Qu, Q. Zou, J. Li, H. Tan, L. Liu, D. Fan and H. Zhang, "Two-dimensional Mxene (Ti3C2)-integrated cellulose hydrogels: toward smart three-dimensional network nanoplatforms exhibiting light-induced swelling and bimodal photothermal/chemotherapy anticancer activity", *ACS Appl. Mater. Interfaces*, 2018, **10**(33), 27631–27643.

25 X. Han, J. Huang, H. Lin, Z. Wang, P. Li and Y. Chen, "2D ultrathin Mxene-based drug-delivery nanoplatform for synergistic photothermal ablation and chemotherapy of cancer", *Adv. Healthcare Mater.*, 2018, **7**(9), 1701394.

26 G. Liu, J. Zou, Q. Tang, X. Yang, Y. Zhang, Q. Zhang, W. Huang, P. Chen, J. Shao and X. Dong, "Surface modified Ti3C2 MXene nanosheets for tumor targeting photothermal/photodynamic/chemo synergistic therapy", *ACS Appl. Mater. Interfaces*, 2017, **9**(46), 40077–40086.

27 B. Zhu, J. Shi, C. Liu, J. Li and S. Cao, "In-situ self-assembly of sandwich-like Ti3C2 MXene/gold nanorods nanosheets for synergistically enhanced near-infrared responsive drug delivery", *Ceram. Int.*, 2021, **47**(17), 24252–24261.

28 Y. Liu, Q. Han, W. Yang, X. Gan, Y. Yang, K. Xie, L. Xie and Y. Deng, "Two-dimensional MXene/cobalt nanowire heterojunction for controlled drug delivery and chemo-photothermal therapy", *Mater. Sci. Eng. C.*, 2020, **116**, 111212.

29 Z. Bai, L. Zhao, H. Feng, H. Xu, N. Zhang, Y. Li, J. Song, Y. Bai, R. Yang and F. Feng, "Fabricating Aptamer-functionalized Ti3C2 therapeutic nanoplatform for targeted chemo-photothermal therapy of cancer", *Mater. Des.*, 2023, **226**, 111656.

30 D. B. Longley, D. P. Harkin and P. G. Johnston, "5-fluorouracil: mechanisms of action and clinical strategies", *Nat. Rev. Cancer*, 2003, **3**(5), 330–338.

31 G. Kresse and D. Joubert, "From ultrasoft pseudopotentials to the projector augmented-wave method", *Phys. Rev. B: Condens. Matter Mater. Phys.*, 1999, **59**(3), 1758.

32 J. P. Perdew, K. Burke and M. Ernzerhof, "Generalized gradient approximation made simple", *Phys. Rev. Lett.*, 1996, **77**(18), 3865.

33 S. Grimme, "Accurate description of van der Waals complexes by density functional theory including empirical corrections", *J. Comput. Chem.*, 2004, **25**(12), 1463–1473.

34 S. Grimme, "Semiempirical GGA-type density functional constructed with a long-range dispersion correction", *J. Comput. Chem.*, 2006, **27**(15), 1787–1799.
35 F. Wu, K. Luo, C. Huang, W. Wu, P. Meng, Y. Liu and E. Kan, "Theoretical understanding of magnetic and electronic structures of Ti3C2 monolayer and its derivatives", *Solid State Commun.*, 2015, **222**, 9–13.
36 M. Faraji, A. Bafekry, M. M. Fadlallah, F. Molaei, N. N. Hieu, P. Qian, M. Ghergherehchi and D. Gogova, "Surface modification of titanium carbide MXene monolayers (Ti_2C and Ti_3C_2) *via* chalcogenide and halogenide atoms", *Phys. Chem. Chem. Phys.*, 2021, **23**(28), 15319–15328.
37 Q. Meng, J. Ma, Y. Zhang, Z. Li, C. Zhi, A. Hu and J. Fan, "The S-functionalized Ti 3 C 2 Mxene as a high capacity electrode material for Na-ion batteries: a DFT study", *Nanoscale*, 2018, **10**(7), 3385–3392.
38 M. Iqbal, J. Fatheema, Q. Noor, M. Rani, M. Mumtaz, R. K. Zheng, S. A. Khan and S. Rizwan, "Co-existence of magnetic phases in two-dimensional MXene", *Mater. Today Chem.*, 2020, **16**, 100271.
39 I. R. Shein and A. L. Ivanovskii, "Graphene-like titanium carbides and nitrides Tin+ 1Cn, Tin+ 1Nn (n= 1, 2, and 3) from de-intercalated MAX phases: First-principles probing of their structural, electronic properties and relative stability", *Comput. Mater. Sci.*, 2012, **65**, 104–114.
40 H. Gholivand, S. Fuladi, Z. Hemmat, A. Salehi-Khojin and F. Khalili-Araghi, "Effect of surface termination on the lattice thermal conductivity of monolayer Ti3C2Tz MXenes", *J. Appl. Phys.*, 2019, **126**(6), 065101.
41 M. Kurtoglu, M. Naguib, Y. Gogotsi and M. W. Barsoum, "First principles study of two-dimensional early transition metal carbides", *MRS Commun.*, 2012, **2**, 133–137.
42 S. Rafiq, S. Awan, R. K. Zheng, Z. Wen, M. Rani, D. Akinwande and S. Rizwan, "Novel room-temperature ferromagnetism in Gd-doped 2-dimensional Ti3C2Tx MXene semiconductor for spintronics", *J. Magn. Magn. Mater.*, 2020, **497**, 165954.
43 O. Mashtalir, M. Naguib, V. N. Mochalin, Y. Dall'Agnese, M. Heon, M. W. Barsoum and Y. Gogotsi, "Intercalation and delamination of layered carbides and carbonitrides", *Nat. Commun.*, 2013, **4**(1), 1716.
44 K. L. Firestein, J. E. von Treifeldt, D. G. Kvashnin, J. F. Fernando, C. Zhang, A. G. Kvashnin, E. V. Podryabinkin, A. V. Shapeev, D. P. Siriwardena, P. B. Sorokin and D. Golberg, "Young's modulus and tensile strength of Ti3C2 MXene nanosheets as revealed by *in situ* TEM probing, AFM nanomechanical mapping, and theoretical calculations", *Nano Lett.*, 2020, **20**(8), 5900–5908.
45 R. G. Parr and R. G. Pearson, "Absolute hardness: companion parameter to absolute electronegativity", *J. Am. Chem. Soc.*, 1983, **105**(26), 7512–7516.
46 N. Zhang, Y. Hong, S. Yazdanparast and M. A. Zaeem, "Superior structural, elastic and electronic properties of 2D titanium nitride MXenes over carbide MXenes: a comprehensive first principles study", *2D Mater.*, 2018, **5**(4), 045004.
47 Q. Tang, Z. Zhou and P. Shen, "Are MXenes promising anode materials for Li ion batteries? Computational studies on electronic properties and Li storage capability of Ti3C2 and Ti3C2X2 (X= F, OH) monolayer", *J. Am. Chem. Soc.*, 2012, **134**(40), 16909–16916.
48 G. R. Berdiyorov, "Optical properties of functionalized Ti3C2T2 (T= F, O, OH) MXene: First-principles calculations", *AIP Adv.*, 2016, **6**(5), 055105.
49 H. Yekeler and D. Özbakır, "Concerning the solvent effect in the tautomerism of uracil, 5-fluorouracil, and thymine by density-functional theory and *ab initio* calculations", *J. Mol. Model.*, 2001, **7**, 103–111.
50 A. Yaraghi, O. M. Ozkendir and M. Mirzaei, "DFT studies of 5-fluorouracil tautomers on a silicon graphene nanosheet", *Superlattices Microstruct.*, 2015, **85**, 784–788.
51 B. Blicharska and T. Kupka, "Theoretical DFT and experimental NMR studies on uracil and 5-fluorouracil", *J. Mol. Struct.*, 2002, **613**(1–3), 153–166.
52 M. B. Javan, A. Soltani, Z. Azmoodeh, N. Abdolahi and N. Gholami, "A DFT study on the interaction between 5-fluorouracil and B 12 N 12 nanocluster", *RSC Adv.*, 2016, **6**(106), 104513–104521.
53 H. Othmani, R. Ben Said, N. Terzi, N. E. Jaidane, M. Mogren Al Mogren, A. Elmarghany and M. Hochlaf, "Structural, energetic and spectroscopic characterisation of 5-fluorouracil anticarcinogenic drug isomers, tautomers and ions", *Mol. Phys.*, 2019, **117**(13), 1589–1603.
54 H. Li, A. Li, D. Zhang, Q. Wu, P. Mao, Y. Qiu, Z. Zhao, P. Yu, X. Su and M. Bai, "First-Principles Study on the Structural, Electronic, and Lithium Storage Properties of Ti3C2T2 (T= O, F, H, OH) MXene", *ACS Omega*, 2022, **7**(44), 40578–40585.
55 T. Ahmed, M. A. Rahman, R. Islam, A. A. Piya and S. U. D. Shamim, "Unravelling the adsorption performance of BN, AlN, GaN and InN 2D nanosheets towards the ciclopirox, 5-fluorouracil and nitrosourea for anticancer drug delivery motive: A DFT-D with QTAIM, PCM and COSMO investigations", *Comput. Theor. Chem.*, 2022, **1214**, 113797.
56 M. K. Hazrati, Z. Javanshir and Z. Bagheri, "B24N24 fullerene as a carrier for 5-fluorouracil anti-cancer drug delivery: DFT studies", *J. Mol. Graphics Modell.*, 2017, **77**, 17–24.
57 M. H. Mohammed and F. H. Hanoon, "Application of zinc oxide nanosheet in various anticancer drugs delivery: quantum chemical study", *Inorg. Chem. Commun.*, 2021, **127**, 108522.
58 N. Ershadi, R. Safaiee and M. M. Golshan, "Functionalized (4, 0) or (8, 0) SWCNT as novel carriers of the anticancer drug 5-FU; a first-principle investigation", *Appl. Surf. Sci.*, 2021, **536**, 147718.
59 K. Shayan and A. Nowroozi, "Boron nitride nanotubes for delivery of 5-fluorouracil as anticancer drug: a theoretical study", *Appl. Surf. Sci.*, 2018, **428**, 500–513.
60 A. Soltani, M. T. Baei, E. T. Lemeski, S. Kaveh and H. Balakheyli, "A DFT study of 5-fluorouracil adsorption on the pure and doped BN nanotubes", *J. Phys. Chem. Solids*, 2015, **86**, 57–64.

61 F. Safdari, H. Raissi, M. Shahabi and M. Zaboli, "DFT calculations and molecular dynamics simulation study on the adsorption of 5-fluorouracil anticancer drug on graphene oxide nanosheet as a drug delivery vehicle", *J. Inorg. Organomet. Polym. Mater.*, 2017, **27**, 805–817.
62 N. Wazzan, K. A. Soliman and W. A. Halim, "Theoretical study of gallium nitride nanocage as a carrier for 5-fluorouracil anticancer drug", *J. Mol. Model.*, 2019, **25**, 1–19.
63 M. H. Mohammed and F. H. Hanoon, "Theoretical prediction of delivery and adsorption of various anticancer drugs into pristine and metal-doped graphene nanosheet", *Chin. J. Phys.*, 2020, **68**, 578–595.
64 R. G. Parr, R. A. Donnelly, M. Levy and W. E. Palke, "Electronegativity: the density functional viewpoint", *J. Chem. Phys.*, 1978, **68**(8), 3801–3807.
65 S. Zhao, W. Kang and J. Xue, "MXene nanoribbons", *J. Mater. Chem. C*, 2015, **3**(4), 879–888.
66 J. Fatheema, M. Fatima, N. B. Monir, S. A. Khan and S. Rizwan, "A comprehensive computational and experimental analysis of stable ferromagnetism in layered 2D Nb-doped Ti3C2 MXene", *Phys. E*, 2020, **124**, 114253.
67 A. Adnan, R. Lam, H. Chen, J. Lee, D. J. Schaffer, A. S. Barnard, G. C. Schatz, D. Ho and W. K. Liu, "Atomistic simulation and measurement of pH dependent cancer therapeutic interactions with nanodiamond carrier", *Mol. Pharmaceutics*, 2011, **8**(2), 368–374.
68 M. Rouhani, "Density functional theory study towards capability of Ga-doped boron nitride nanosheet as a nanocarrier for 3-allyl-2 selenohydantoin anticancer drug delivery", *Phys. E*, 2021, **126**, 114437.